Journal of The Electrochemical Society, **164** (4) A754-A759 (2017)
0013-4651/2017/164(4)/A754/6/$37.00 © The Electrochemical Society

Estimation of State-of-Charge for Zinc-Bromine Flow Batteries by In Situ Raman Spectroscopy

Hyun Ju Lee,[a,b] Dong-Won Kim,[b] and Jung Hoon Yang[a,c,z]

[a]*Conversion Materials Laboratory, Korea Institute of Energy Research, Daejeon 34129, South Korea*
[b]*Department of Chemical Engineering, Hanyang University, Seoul 04763, South Korea*
[c]*Department of Renewable Energy Engineering, University of Science and Technology, Daejeon 34113, South Korea*

A zinc–bromine redox flow battery (ZBB) has attracted increasing attention as a potential energy-storage system because of its cost-effectiveness and high energy density. However, its aqueous zinc bromide phase and non-aqueous polybromide phase are inhomogeneously mixed in the positive electrolyte. Furthermore, various equilibrium reactions, e.g., charge-transfer reactions, polybromide formation, and complexation, simultaneously occur in the battery. Because of these complex reactions, it is difficult to systematically analyze its electrolyte, which a component crucial for the stable operation of the battery. Especially, although the state-of-charge (SoC) of an electrolyte is crucial for preventing overcharging or discharging and side reactions, its accurate estimation is difficult. As a result, there have been few studies on estimation of the SoC in ZBBs. In this study, in situ Raman spectroscopy is employed for the real-time estimation of the SoC in 25 charge–discharge cycles. To exclude errors arising from the inhomogeneous dispersion of the non-aqueous phase, SoC is monitored on the negative electrolyte. External standard solutions are measured, and the calibration curve is constructed just before in situ measurements at every cycle to minimize instrumental errors, e.g., those caused by alignment. This in situ methodology exhibits high accuracy and reproducibility.

Manuscript submitted December 15, 2016; revised manuscript received January 20, 2017. Published February 16, 2017.

To solve air pollution arising from the use of traditional fossil fuels, tremendous investment has been made toward the development of facilities producing renewable energy, e.g., solar and wind power plants. These non-hydro renewable sources have rapidly grown, with a sevenfold increase over the last decade. By 2030, these renewable sources have been estimated to supply approximately 25% of the global electricity.[1,2] With the gradual increase in the proportion of renewable energy, the efficient management of the surplus energy produced during peak times has emerged as a significant task because of its weather- and time-dependent nature. Hence, approaches for storing this surplus energy are crucial to projects generating clean energy. To address this challenge, stationary energy-storage systems in the form of large-scale facilities are required. A redox flow battery (RFB) is one of the most economical systems for large-scale energy storage, with several advantages of cost-effectiveness, long service life, rapid response, and independent cell design for power and energy capacity.

The zinc–bromine RFB (ZBB) is one of the most cost-competitive RFBs because of its low electrolyte cost and high energy density (70 $Wh \cdot kg^{-1}$).[3,4] This flow battery employs the Zn/Zn^{2+} and Br/Br^{-} redox reaction:

$2Br^{-} \leftrightarrow Br_2 + 2e^{-}$ ($E^0 = 1.07$ V vs. SHE) at the positive electrode

$Zn^{2+} + 2e^{-} \leftrightarrow Zn$ ($E^0 = -0.76$ V vs. SHE) at the negative electrode

Typically, several quaternary ammonium compounds in the electrolyte are used to capture bromine molecules produced at the positive electrode during charging.[5–7] Although these compounds are initially soluble in an aqueous solution, they form a non-aqueous polybromide complex phase after bromine capture. This reaction results in an aqueous zinc bromide phase and a non-aqueous polybromide phase, leading to a positive electrolyte having a complicated composition. This complex composition poses difficulties in the systematic analysis of an electrolyte, which is a component crucial to the stable operation of the flow battery.

Especially, although the state-of-charge (SoC) of the electrolyte is crucial for preventing the overcharge or discharge and side reactions, it is difficult to accurately estimate the SoC in the ZBB. For a vanadium RFB, various approaches, such as electrolyte conductivity measurement,[8,9] spectrophotometric analysis,[10–13] and open-circuit voltage (OCV) method,[14,15] have been adopted for the real-time monitoring of the SoC of the electrolyte. Measurement of conductivity is based on its linear variation with the SoC. This approach is strongly dependent on the total ion concentration of the electrolyte. However, it is nonselective with respect to type of charge-carrying ions, e.g., vanadium ion and proton. Thus, this method does not provide precise information on the concentration of redox-active species without also knowing the concentration of protons, which is affected by side reactions such as hydrogen evolution. The use of UV–vis spectrophotometric analysis for the SoC monitoring of a vanadium electrolyte has also been proposed previously.[10–13] It is a straightforward approach for measuring the actual concentrations of redox-active species based on the absorbance of four vanadium species (V^{2+}, V^{3+}, VO^{2+}, and VO_2^{+}) at different wavelengths. By using Beer's law, the vanadium concentration in solution can be determined:

$$I = I_0 \exp(-\sigma C d), \quad [1]$$

where I_0 and I are the intensities of the incident light and the light transmitted through the material, respectively. σ is the molar absorption coefficient, d is the thickness of the absorber layer, and C is the molar concentration. However, performing online SoC monitoring by this method is difficult because of the extremely high absorption intensities measured. This necessitates the dilution of the solution prior to spectral measurements. Zhang et al. have reported the transmittance spectra of the vanadium electrolyte in real time during charge–discharge tests by decreasing the absorption channel thickness to 0.5 mm.[13]

The OCV method, the most commonly used method for real-time SoC estimation, is simple. The SoC of the battery can be measured from the OCV by applying the Nernst equation:

$$E = E^{0\prime} + \frac{RT}{F} \ln\left(\frac{C_{VO_2^+} \cdot C_{V^{2+}} \cdot (C_{H^+}^{+})^3}{C_{VO^{2+}} \cdot C_{V^{3+}} \cdot C_{H^+}^{-}}\right), \quad [2]$$

where E is the potential difference, $E^{0\prime}$ is the formal reduction potential, R is the universal gas constant, T is the absolute temperature, and C is the concentration of each species. Superscripts + and − represent the positive and negative half-cells, respectively. This method assumes that the two half-cell solutions are well balanced.

Measuring the SoC for the vanadium RFB is relatively easy because of its simple charge-transfer reaction between redox-active species. In contrast, various equilibrium reactions, e.g., charge-transfer reaction,[6,16] polybromide (Br^{-}, Br_3^{-} Br_5^{-} and Br^{7-}) formation,[17] and complexation,[18,19] simultaneously occur in the ZBB. Furthermore, the reactants and products of the redox reaction exist in separate phases. For example, the zinc ions in the aqueous phase are reduced during charging and then electrodeposited on the zinc metal

[z]E-mail: enviroma@kier.re.kr

solid phase on the negative electrode. During this stage, bromide ions in the aqueous phase are oxidized to bromine, which is captured by quaternary ammonium compounds and then converted into the non-aqueous polybromide complex phase. As the Nernst equation is based on the thermodynamic equilibrium between the reactant and product, we cannot obtain the actual OCV reflecting the precise concentrations of both reactant and product. For these reasons, there have been few studies on estimating the SoC of ZBBs.

Zinc and bromide ions form various zinc bromide complexes in the aqueous phase, such as $ZnBr^+$, $ZnBr_2$, $ZnBr_3^-$, and $ZnBr_4^{2-}$. Several studies have reported Raman band locations for these complexes.[20–23] Using Raman spectra, Pell has found that the concentrations of $ZnBr_2$, $ZnBr_3^-$, and $ZnBr_4^{2-}$ complexes are a function of temperature and the SoC of the battery.[23] However, no clear trends were observed in the individual Raman intensities with respect to the SoC.

In this study, a strong linear relation between the Raman band intensity and total zinc bromide concentration is observed. On the basis of this result, Raman spectroscopy is found to be effective for the real-time SoC estimation of ZBB. To avoid errors arising from the inhomogeneous mixing of the aqueous and non-aqueous phases in the positive electrolyte, in situ Raman analysis is performed on the negative electrolyte. Using a crossover test, we observed a rapid concentration equilibrium established through a porous separator between the negative and positive aqueous phases. Raman spectroscopy was carried out on the electrolyte flowing from the cell to the reservoir during the charge–discharge. The accuracy of SoC estimation based on this spectrometric measurement was also determined.

Experimental

Raman spectroscopy.—Raman spectral analysis was conducted using a DXR Raman microscope (Thermo Fisher Scientific Inc.). Instrumentation conditions were as follows: laser wavelength of 532 nm, spectral range of 100 to 3400 cm^{-1}, sample exposure time of 2 s, with a total of 60 sample exposures. To determine the linear relationship between the concentration and Raman intensity, Raman spectra were recorded for 0.1 to 2.5 M solutions of $ZnBr_2$ (98%, Alfa Aesar) and 0.1 to 0.8 M solutions of 1-ethyl-1-methylpyrrolidinium bromide (MEP-Br; 99%, Sigma Aldrich).

For in situ Raman spectroscopy, a fiber optic probe and a cuvette cell (10 × 10 mm; 130-QS, Hellma Inc.) through which the electrolyte can flow were employed (Figure S1). The Raman probe and cuvette were used in a dark room. To minimize instrumental errors such as those caused by alignment and to quantitatively interpret the results, external standard solutions were analyzed, and the calibration curve was obtained right before the in situ measurement at every cycle. Standard solutions were prepared by charging ZBB electrolytes to the predetermined SoCs (0%, 10%, 20%, 30%, and 40%) in separate single cells and storing the negative electrolyte in separate sealed cuvettes.

Crossover test.—To measure the permeability to $ZnBr_2$ and MEP-Br of the porous separator between the negative and positive electrolytes, crossover tests were conducted. For the crossover test, the manifold structure, separator, and graphite plates of the cells were the same as those used for the single cells in the charge–discharge tests. For the $ZnBr_2$ crossover test, 2.25 and 1.0 M $ZnBr_2$ solutions were used as the concentrated and dilute solutions, respectively. For the MEP-Br crossover test, 0.8 and 0.4 M MEP-Br solutions were used as the concentrated and dilute solutions, respectively. The solutions were circulated at a flow rate of 100 mL · min^{-1}. The crossover rate is expressed as follows:

$$V\frac{\partial C_D(t)}{\partial t} = A\frac{P}{L}\left(C_C(t) - C_D(t)\right) = A\frac{P}{L}\left(C_{C0} + C_{D0} - 2C_D(t)\right) \quad [3]$$

$$\frac{V \cdot L}{2A} \cdot \ln\left(\frac{C_{C0} - C_{D0}}{C_{C0} + C_{D0} - 2C_D(t)}\right) = P \cdot t, \quad [4]$$

where C_C and C_D are the concentrations of the species in the concentrated and dilute solutions, respectively. C_{C0} and C_{D0} are the initial concentrations of the species in the concentrated and dilute solutions, respectively. A and L are the area and thickness of the separator, respectively. P is the permeability of the species, and V is the volume of the dilute solution. Hence, the permeability is obtained by plotting the left term of Equation 4 as a function of time.

Charge–discharge experiments.—Each charge–discharge experiment was performed in a single flow cell with an active electrode area of 35 cm^2 (7.0 cm × 5.0 cm). A single cell consists of graphite bipolar plates, a porous separator (Asahi Kasei Co., Ltd., Japan), a polyethylene mesh, and polytetrafluoroethylene flow frames. Graphite bipolar electrodes without and with an activated carbon layer were used as the negative and positive electrodes, respectively.

The initial negative and positive electrolytes had the same composition (2.25 M $ZnBr_2$, 0.5 M $ZnCl_2$, 5 mL · L^{-1} bromine, and 0.8 M MEP-Br in deionized water). An electrolyte with a volume of 30 mL was circulated at a flow rate of 100 mL · min^{-1} using peristaltic pumps.

This single flow cell was charged to a previously determined capacity (2.88 Ah), corresponding to 40% SoC, and then discharged to 0.1 V at a current density of 20 mA · cm^{-2} using a Maccor series 4000 Battery testing system. Experiments were performed at room temperature (22 ± 1°C).

Results and Discussion

Raman spectra for the zinc bromide electrolyte.—Raman spectral peaks of the individual species constituting the electrolyte were observed between 100 and 3400 cm^{-1} (Figure 1a). Peaks corresponding to zinc bromide species in the aqueous 1.5 M zinc bromide solution were observed from 150 to 250 cm^{-1}, which is in agreement with previously reported studies.[20–23] Zinc bromide is present as various soluble complexes, e.g., $ZnBr^+$, $ZnBr_2$, $ZnBr_3^-$, and $ZnBr_4^{2-}$. Previously, Pell has observed vibrational bands of these complexes at approximately 240, 205, 183, and 170 cm^{-1}, respectively.[23] In this study, two peaks corresponding to $ZnBr_2$ and $ZnBr_3^-$ species (approximately 198 and 183 cm^{-1}, respectively) were clearly observed.

For the 0.025 M MEP-Br solution, the vibrational bands were characterized by several small peaks at 300–1500 cm^{-1} and a prominent peak at approximately 2994 cm^{-1}. Hence, its bands do not overlap with those of zinc bromide.

During charging, bromide ions are oxidized to bromine on the positive electrode. MEP-Br captures the bromine and then forms the MEP-Br_x polybromide phase. This phase is clearly separated from the aqueous electrolyte because of its strong hydrophobicity. The non-aqueous MEP-Br_x phase is obtained by charging the ZBB electrolyte in the single cell to 40% SoC, withdrawing the positive electrolyte, and then separating it from the aqueous phase. The Raman spectrum observed for MEP-Br_x was different from that of aqueous MEP-Br: the peak at approximately 2994 cm^{-1} shifted to 3050 cm^{-1}, and a new, sharp peak was observed at around 257 cm^{-1}.

To investigate spectral changes in the positive electrolyte with the SoC, a quartz cell was installed on the circulation line of the positive electrolyte, placing it in close contact with the in situ Raman probe (Figure S1). While the single cell was charged to 40% SoC, Raman spectra were collected and analyzed for the positive electrolyte at 0%, 13.3%, 26.7%, and 40.0% SoC (Figure 1b). Distinct zinc bromide peaks were observed at approximately 198 cm^{-1} at 0% SoC. With increasing SoC, these peaks gradually shifted to 257 cm^{-1}, indicative of the formation of the MEP-Br_x polybromide phase. This shift is caused by the oxidation of the bromide ions to bromine and the subsequent capture of bromine by MEP-Br. Meanwhile, the aqueous MEP-Br peak at around 2994 cm^{-1} decreased and the non-aqueous MEP-Br_x peak at around 3050 cm^{-1} increased.

All vibrational bands for zinc bromide, MEP-Br, and MEP-Br_x in the positive electrolyte were observed because non-aqueous MEP-Br_x was dispersed in the aqueous zinc bromide and MEP-Br solutions.

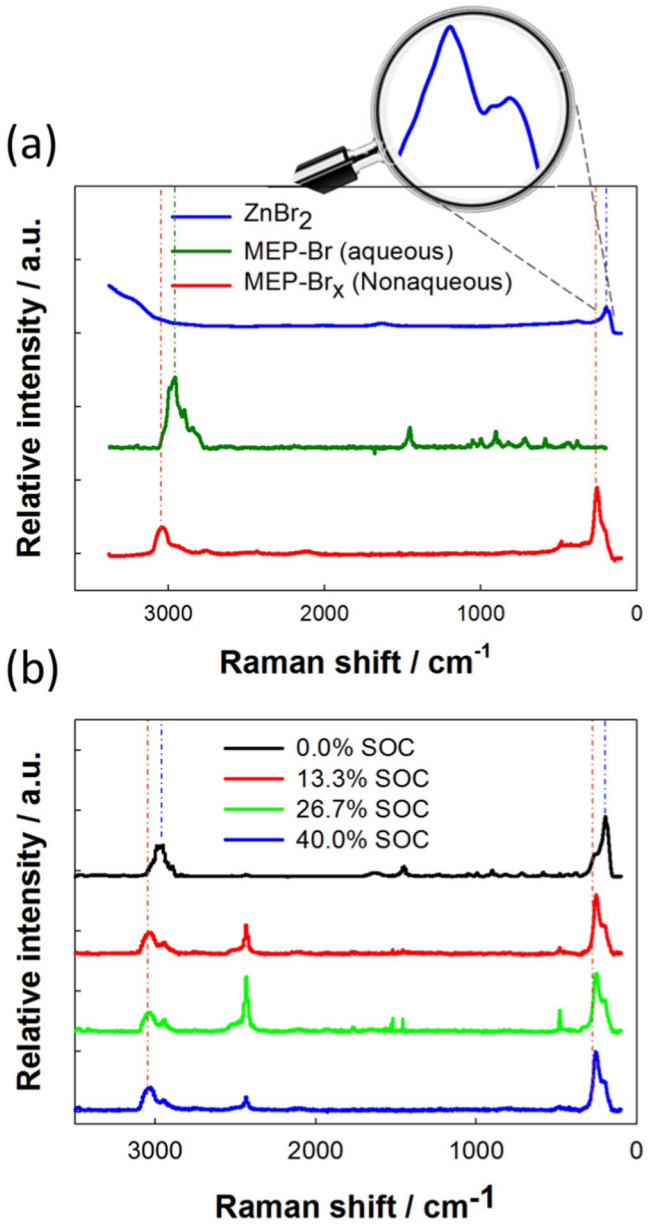

Figure 1. (a) Raman spectra of 1.5 M zinc bromide, 0.025 M MEP-Br, and MEP-Br_x polybromide complex solutions at 100 to 3400 cm^{-1}. The MEP-Br_x solution was obtained by charging the ZBB electrolyte to 40% SoC and separating it from the aqueous phase. (b) Raman spectra for the positive electrolyte at different SoCs. While the single cell was charged to 40% SoC, Raman spectra were collected and analyzed at 0%, 13.3%, 26.7%, and 40.0% SoC.

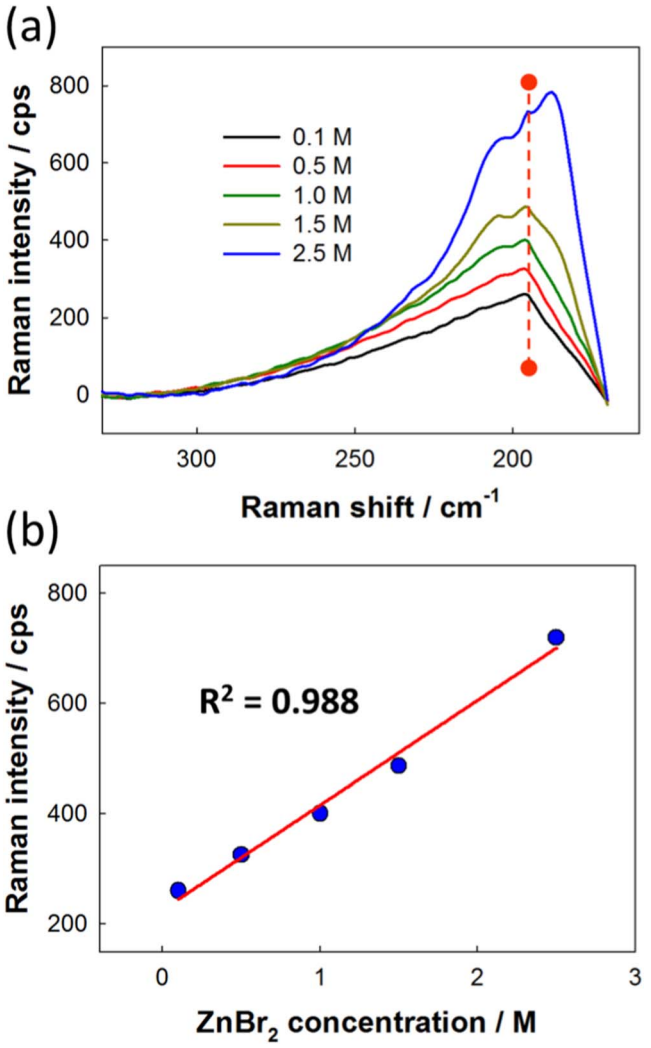

Figure 2. (a) Raman spectra for different concentrations of zinc bromide. Zinc bromide was dissolved in the concentration range of 0.1 to 2.5 M in deionized water. The spectra were collected using a fiber optic probe and a cuvette cell. (b) Raman peak intensity at 198 cm^{-1} as a function of $ZnBr_2$ concentration.

However, the spectra exhibited marginal differences from 13.3% to 40.0% SoC, possibly caused by the inhomogeneous dispersion of the non-aqueous MEP-Br_x phase and contamination of the quartz cell window by the phase upon its formation. Therefore, quantitatively analyzing the Raman spectral characteristics of the positive electrolyte as a function of the SoC is difficult. To exclude the effect of inhomogeneous dispersion of the non-aqueous MEP-Br_x phase, Raman spectroscopy of the negative electrolyte was carried out.

SoC estimation by Raman spectroscopy of the negative electrolyte.—Figure 2a shows the Raman spectra of the zinc bromide solutions at different concentrations. Symmetric stretching vibrations of $ZnBr^+$, $ZnBr_2$, $ZnBr_3^-$, and $ZnBr_4^{2-}$ overlapped, making it difficult to resolve their individual vibrational bands. According to Goggin et al., the intensity ratio of the bands is strongly affected by the ratio of bromide to zinc ions and the temperature.[24] During actual ZBB operation, the Br^-/Zn^{2+} ratio was 2, with side reactions, e.g., hydrogen evolution, being neglected. Assuming a constant ratio for the individual vibration bands, the peak intensity at around 198 cm^{-1} as a function of the zinc bromide concentration could be plotted (Figure 2b). The intensity proportionally increased with the zinc bromide concentration, suggesting that the in situ Raman analysis can be used to estimate the SoC in the electrolyte.

Figure S2 shows the Raman spectra for different concentrations of MEP-Br. The peak intensity at approximately 2994 cm^{-1} also exhibited a strong linear relation to the MEP-Br concentration in the range of 0.1 to 0.8 M. However, the Raman sensitivity at concentrations of less than 0.1 M deteriorated, resulting in a broad H_2O peak at greater than 3000 cm^{-1}. As the operation of the ZBB is typically within an SoC range of 0% to 70%, corresponding to MEP-Br concentrations of 0.80 to 0.24 M, this Raman peak at approximately 2994 cm^{-1} can be used to estimate the SoC.

To estimate the real-time SoC for the entire battery based on the Raman spectral analysis of the negative electrolyte, the concentrations of $ZnBr_2$ and MEP-Br in the negative electrolyte are assumed to be the same as those in the aqueous phase of the positive electrolyte because of their rapid exchange through the porous separator. To verify this assumption, a crossover test was carried out for the two species. The

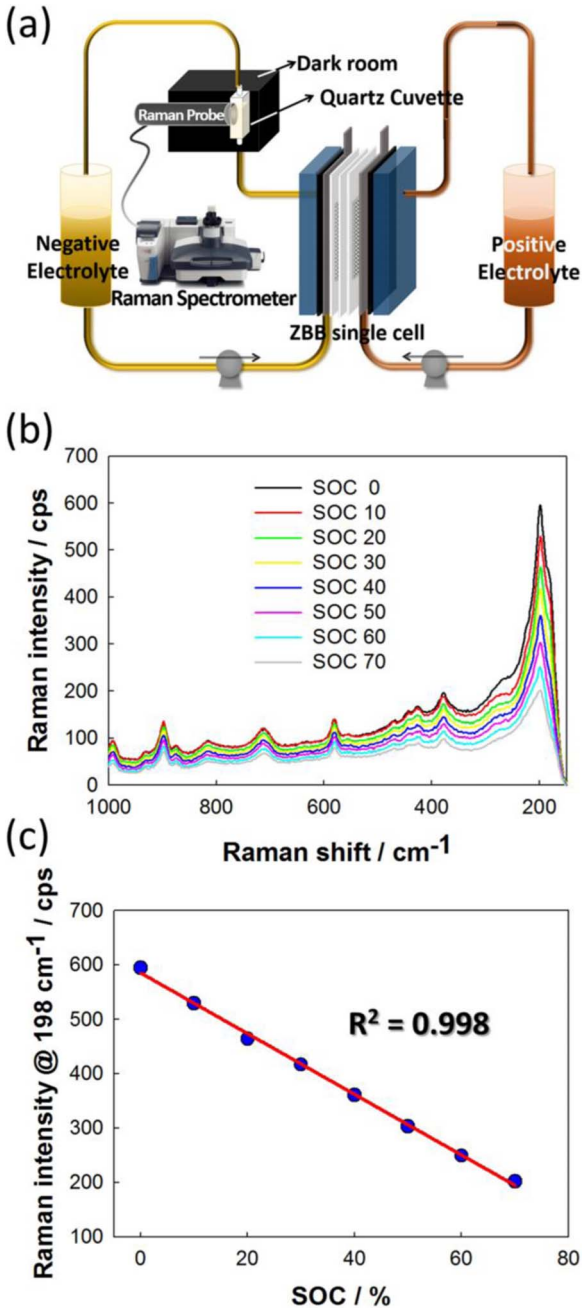

Figure 3. (a) Schematic of the apparatus and single cell used for in situ Raman spectroscopy. A quartz cell was installed on the circulation line of the negative electrolyte, placing it in close contact with the in situ Raman probe. (b) Raman spectra for the negative electrolyte at different SoCs. While the single cell was charged to 70% SoC, Raman spectra were collected and analyzed at 0%, 10.0%, 20.0%, 30.0%, 40.0%, 50.0%, 60.0%, and 70.0% SoC. (c) Raman peak intensity at 198 cm^{-1} as a function of SoC.

concentration of the dilute solution as a function of time was monitored (Figure S3). The calculated permeabilities to $ZnBr_2$ and MEP-Br were 4.11×10^{-6} and 1.29×10^{-6} $cm^2 \cdot s^{-1}$, respectively. Zinc and bromide ions passed through the separator more easily than MEP^+ because of their smaller ionic size, indicating that $ZnBr_2$ satisfies the above assumption better than MEP-Br.

To investigate the spectral change in the negative electrolyte at various SoCs, a quartz cell was installed on the circulation line of the negative electrolyte, placing it in close contact with the in situ Raman probe (Figure 3a). The ZBB electrolyte was charged to 70% SoC, and Raman spectroscopy was performed at 0%, 10%, 20%, 30%, 40%, 50%, 60%, and 70% SoC (Figure 3b). With increasing SoC, the zinc bromide concentration in the negative electrolyte decreased, and the corresponding peak intensity declined with a constant slope (Figure 3c). Raman analysis on the negative side remained unaffected by the non-aqueous polybromide phase and exhibited strong proportionality as a function of SoC, which is opposite to results observed for the positive side. However, the peak intensity for MEP-Br deviated from linearity in the low SoC range (Figure S4). This result can be explained by its low permeability and slow concentration equilibrium between the negative electrolyte and the aqueous phase of the positive electrolyte. Furthermore, the consumption rate of the aqueous MEP-Br may not be a linear function of SoC, especially in the low SoC range. Hence, the Raman band for $ZnBr_2$ is a more appropriate tool as compared to MEP-Br for estimating SoC.

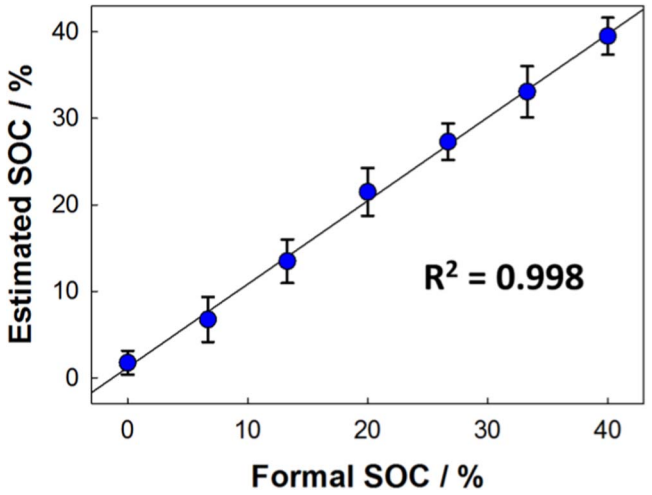

Figure 4. Comparison between the estimated SoC and the formal SoC for the first cycle. The formal SoC was calculated from the charge capacity applied during every cycle. It was assumed to be 0% at the end of discharge process even though the cell was not completely discharged. The estimated SoC was calculated from the present zinc bromide concentration of the negative electrolyte, which was converted from the Raman peak intensity at 198 cm^{-1}.

Real-time SoC estimation during charge–discharge.—To examine the accuracy of the proposed SoC estimation, in situ Raman analysis was conducted for three charge–discharge experiments. To quantitatively interpret the Raman results, external standard solutions were analyzed, and the calibration curve was obtained before the in situ measurement at every cycle. The peak intensity at around 198 cm^{-1} was converted to the zinc bromide concentration through the calibration curve. Estimation of the actual SoC of the electrolyte was based on the calculated concentration of zinc bromide:

$$\text{Estimated SoC} = 1 - \frac{\text{Calculated concentration of zinc bromide}}{\text{Initial concentration of zinc bromide}}$$

The estimated SoCs were compared to the formal SoCs obtained for the first cycle (Figure 4). The formal SoC was calculated from the charge capacity applied during every cycle. It was assumed to be 0% at the end of discharge process even though the cell was not completely discharged. The estimated SoC almost coincided with the formal SoC in the first cycle because the external standard solution was prepared by electrolyzing the electrolyte to the predetermined SoC. It also showed high reproducibility (standard deviation of 2.35%).

Estimated and formal SoCs as a function of the cycle number were also obtained. The charge–discharge test was performed using a single cell for 25 cycles. This experiment did not include an additional stripping process, in which the zinc deposits remaining on the negative electrode at the end of the discharge step dissolve into the electrolyte, and the electrode surface becomes clean and uniform. The residual zinc can cause the uneven formation of zinc dendrites during subsequent charging, which puncture the separator and can

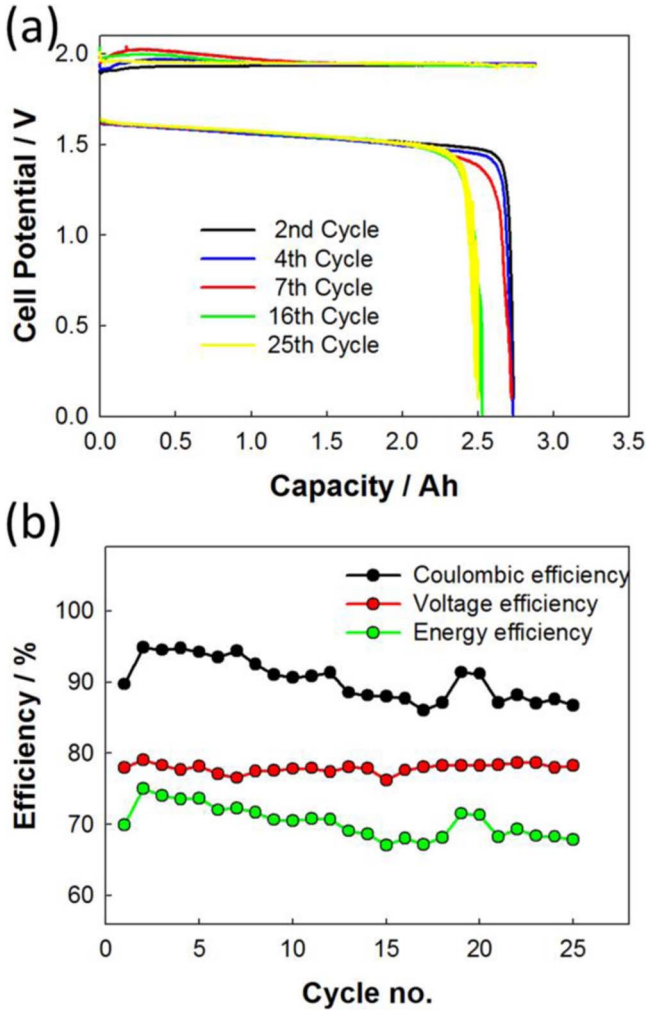

Figure 5. (a) Charge–discharge curves obtained by using a single ZBB at different cycles. This single flow cell was charged to a previously determined capacity (2.88 Ah), corresponding to 40% SoC, and then discharged to 0.1 V at a current density of 20 mA · cm^{-2}. An electrolyte with a volume of 30 mL was circulated at a flow rate of 100 mL · min^{-1} using peristaltic pumps. (b) Coulombic, voltage, and energy efficiencies as a function of cycle number.

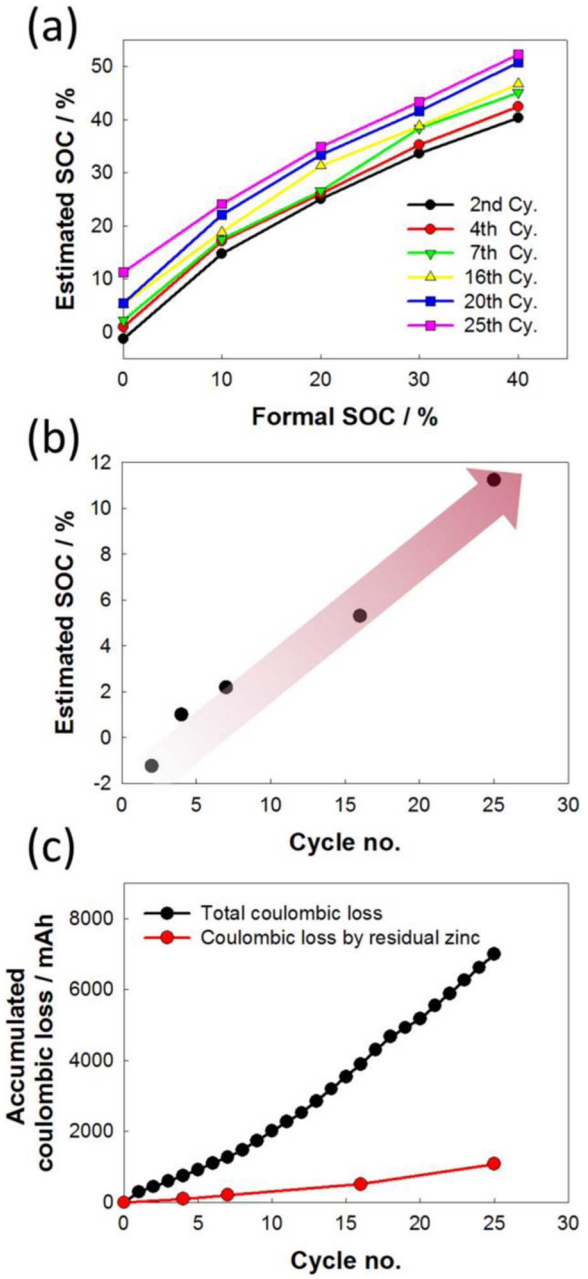

Figure 6. (a) Estimated SoCs calculated from in situ Raman spectral measurement versus formal SoCs. While the single cell was operated during 25 cycles, the Raman spectra were collected and analyzed on the charging step of 2nd, 4th, 7th, 16th, 20th, and 25th cycles. (b) Variation of estimated SoCs at 0% formal SoC with the cycle number. (c) Total accumulated coulombic loss and the coulombic loss caused by residual zinc. The accumulated coulombic loss was calculated from the difference between the charge and discharge capacities. The coulombic loss caused by the residual zinc on the negative electrode was also calculated from the concentration of the present zinc bromide of the negative electrolyte, which was converted from the Raman peak intensity at 198 cm^{-1}.

lead to severe self-discharge.[23,25,26] The discharge capacity gradually decreased from 2.73 A · h at the 2nd cycle to 2.50 A · h at the 25th cycle (Figure 5a). This decrease may be due to the effect of the accumulated zinc residue on zinc dendrite formation and subsequent self-discharge. This is also indicated by the decreasing coulombic efficiency (Figure 5b). The coulombic efficiency decreased from 94.9% at the 2nd cycle to 86.7% at the 25th cycle, while the voltage efficiency remained relatively constant (77.9 ± 0.63%). Hence, energy efficiency also showed a steady decrease from 75.1% to 67.9%.

During the same period, Raman data for the negative electrode were collected by in situ measurement. Raman analysis was performed at 0.0%, 10.0%, 20.0%, 30.0%, and 40.0% SoC during charging. Figure 6a shows the relationship between the estimated and formal SoCs in each cycle. The estimated SoC proportionally increased with the formal SoC. For instance, with increase in the formal SoC from 0.0% to 40.0%, the estimated SoC at the second cycle increased from −1.2% to 40.3%. In this cycle, the estimated and formal SoCs exhibited marginal difference. However, the estimated SoC shifted to a value greater than the formal SoC with increasing cycle number. The estimated SoC at the 25th cycle increased from 11.2% to 52.2%, while the formal SoC increased from 0.0% to 40.0%. Figure 6b shows the variation of the estimated SoC at 0% formal SoC with the number of cycles. Zinc bromide in the electrolyte is confirmed to be depleted, and the actual SoC gradually increases with the progress of battery operation. The decline in the zinc bromide concentration can be explained by the residual zinc on the negative electrode surface after discharging.

The accumulated coulombic loss during 25 cycles was calculated from the charge and discharge capacities (results are shown in

Figure 6c). This loss may be explained by various causes, e.g., bromine crossover, side reactions, and residual zinc deposits. The coulombic loss caused by the residual zinc on the negative electrode was also calculated from the concentration of the zinc bromide and compared with the total coulombic loss, which amounted to approximately 15.5%. Hence, minimizing this residual zinc deposit can significantly improve the cell performance. Furthermore, accurate monitoring of the actual SoC and the accumulated residual zinc deposit is necessary because residual zinc possibly results in the formation of zinc dendrites, ultimately leading to cell failure. The in situ Raman spectroscopic analysis of the negative electrolyte enables highly accurate monitoring of the actual SoC.

Conclusions

In summary, in situ Raman spectroscopic analysis of the ZBB was carried out for the real-time estimation of SoC. The Raman intensity of zinc bromide observed at approximately 198 cm^{-1} was strongly proportional to the zinc bromide concentration and to the SoC of the electrolyte. Using an optical fiber probe, the Raman spectra of the electrolyte was obtained in real time during charge–discharge. However, it was difficult to quantitatively analyze the Raman characteristics of the positive electrolyte as a function of the SoC because of the inhomogeneous dispersion of the non-aqueous polybromide complex phase, which resulted in a significant error. Hence, in situ Raman analysis was performed on the negative electrolyte. The concentration variation of zinc bromide in the negative electrolyte could reflect the actual SoC of the entire battery because the negative electrolyte and aqueous phase of the positive electrolyte exhibited high permeability to zinc and bromide ions. Although the SoC estimate based on the in situ Raman analysis matches the formal SoC in the first cycle, it shifted to a value greater than the formal SoC with increasing cycle number. This change indicated that some residual zinc accumulates on the negative electrode. As the residual zinc can form zinc dendrites and cell failure, the accurate monitoring of the actual SoC and of the accumulated residual zinc deposit is crucial to effect stable battery operation. This study demonstrated that the in situ Raman analysis of the negative electrolyte is a possible valid approach to the highly accurate monitoring of the actual SoC.

Acknowledgments

Financial support by the Grant-in-Aid from the Korea Institute of Energy Technology Evaluation and Planning (Project 20152010103100) is greatly appreciated.

References

1. Renewable 2015 Global Status Report, *REN21*, ISBN 978-3-9815934-6-4 (2015).
2. P. Alotto, M. Guarnieri, and F. Moro, *Renew. Sust. Energ. Rev.*, **29**, 325 (2014).
3. L. Zhang, H. Zhang, Q. Lai, X. Li, and Y. Cheng, *J. Power Sources*, **227**, 41 (2013).
4. G. P. Rajarathnam and A. M. Vassallo, *The Zinc/Bromine Flow Battery: Materials Challenges and Practical Solutions for Technology Advancement*, 1st ed., Springer, Singapore (2016).
5. K. J. Cathro, K. Cedzynska, D. C. Constable, and P. M. Hoobin, *J. Power Sources*, **18**, 349 (1986).
6. J.-D. Jeon, H. S. Yang, J. Shim, H. S. Kim, and J. H. Yang, *Electrochim. Acta*, **127**, 397 (2014).
7. G. P. Rajarathnam, M. E. Easton, M. Schneider, A. F. Masters, T. Maschmeyer, and A. M. Vassallo, *RSC Adv.*, **6**, 27788 (2016).
8. M. Skyllas-Kazacos and M. Kazacos, *J. Power Sources*, **196**, 8822 (2011).
9. K. Ngamsai and A. Arpornwichanop, *J. Power Sources*, **298**, 150 (2015).
10. R. P. Brooker, C. J. Bell, L. J. Bonville, H. R. Kunz, and J. M. Fenton, *J. Electrochem. Soc.*, **162**(4), A608 (2015).
11. C. Petchsingh, N. Quill, J. T. Joyce, D. N. Eidhin, D. Oboroceanu, C. Lenihan, X. Gao, R. P. Lynch, and D. N. Buckley, *J. Electrochem. Soc.*, **163**(1), A5068 (2016).
12. N. Quill, C. Petchsingh, R. P. Lynch, X. Gao, D. Oboroceanu, D. N. Eidhin, M. O'Mahony, C. Lenihan, and D. N. Buckley, *ECS Transactions*, **64**(18), 23 (2015).
13. W. Zhang, L. Liu, and L. Liu, *RSC Adv.*, **5**, 100235 (2015).
14. K. W. Knehr and E. C. Kumbur, *Electrochem. Commun.*, **13**, 342 (2011).
15. K. Ngamsai and A. Arpornwichanop, *J. Power Sources*, **282**, 534 (2015).
16. M. Mastragostino and C. Gramellini, *Electrochim. Acta*, **30**, 373 (1985).
17. G. Bauer, J. Drobits, C. Fabjan, H. Mikosch, and P. Schuster, *J. Electroanal. Chem.*, **427**, 123 (1997).
18. D. J. Eustace, *J. Electrochem. Soc.*, **127**, 528 (1980).
19. S. Park, H. Kim, J. Chae, and J. Chang, *J. Phys. Chem. C*, **120**, 3922 (2016).
20. M. M. Yang, D. A. Crerar, and D. E. Irish, *J. Solution Chem.*, **17**, 751 (1988).
21. K. Mibe, I. Chou, A. J. Anderson, R. A. Mayanovic, and W. A. Bassett, *Chem. Geol.*, **259**, 48 (2009).
22. C. C. Pye, S. M. Black, and W. W. Rudolph, *J. Solution Chem.*, **40**, 1932 (2011).
23. W. Pell, Zinc/bromine battery electrolytes: electrochemical, physicochemical and spectroscopic studies, Ph.D thesis, University of Ottawa (1994).
24. P. L. Goggin, G. Johansson, M. Maeda, and H. Wakita, *Acta Chem. Scand.*, **A38**, 625 (1984).
25. J. H. Yang, H. S. Yang, H. W. Ra, J. Shim, and J.-D. Jeon, *J. Power Sources*, **275**, 294 (2015).
26. H. S. Yang, J. H. Park, H. W. Ra, C.-S. Jin, and J. H. Yang. *J. Power Sources*, **325**, 446 (2016).